Article:
Bones, DL, Plane, JMC and Feng, W (2016) Dissociative Recombination of FeO(+) with Electrons: Implications for Plasma Layers in the Ionosphere. Journal of Physical Chemistry A, 120 (9). pp. 1369-1376. ISSN 1089-5639

https://doi.org/10.1021/acs.jpca.5b04947

Dissociative Recombination of FeO^+ with Electrons: Implications for Plasma Layers in the Ionosphere

D. L. Bones[1], J. M. C. Plane[1*], and W. Feng[1,2]

[1] School of Chemistry, University of Leeds, UK

[2] School of Earth and Environment and the National Centre for Atmospheric Science, University of Leeds, UK

* Corresponding author (j.m.c.plane@leeds.ac.uk)

Submitted to the Journal of Physical Chemistry A

James G. Anderson Festschrift

May 2015

Revised July 2015

Abstract. The dissociative recombination (DR) of FeO^+ ions with electrons has been studied in a flowing afterglow reactor. FeO^+ was generated by the pulsed laser ablation of a solid Fe target, and then entrained in an Ar^+ ion/electron plasma where the absolute electron density was measured using a Langmuir probe. A kinetic model describing gas-phase chemistry and diffusion to the reactor walls was fitted to the experimental data, yielding a DR rate coefficient at 298 K of $k(FeO^+ + e^-) = (5.5 \pm 1.0) \times 10^{-7}$ cm^3 $molecule^{-1}$ s^{-1}, where the quoted uncertainty is at the 2σ level. Fe^+ ions in the lower thermosphere are oxidized by O_3 to FeO^+, and this DR reaction is shown to provide a more important route for neutralizing Fe^+ below 110 km than the radiative/ dielectronic recombination of Fe^+ with electrons. The experimental system was first validated by measuring two other DR reaction rate coefficients: $k(O_2^+ + e^-) = (2.0 \pm 0.4) \times 10^{-7}$ and $k(N_2O^+ + e^-) = (3.3 \pm 0.8) \times 10^{-7}$ cm^3 $molecule^{-1}$ s^{-1}, which are in good agreement with the recent literature.

1. Introduction

The presence of metallic ions in the mesosphere/lower thermosphere (MLT) region between 70 and 140 km has been known for nearly 5 decades. Most measurements have been made by rocket-borne mass spectrometry,[1,2] but Mg^+ has also been observed via solar-pumped resonance fluorescence from a rocket[3] and UV-visible spectrometers on spacecraft.[4,5] Ca^+ ions are also observed by ground-based lidar (laser radar).[6] The source of these metals is the ablation of cosmic dust particles entering the atmosphere, which injects a variety of metals between 70 and 120 km.[7]

Metal ions are produced during ablation by hyperthermal collisions with air molecules, and also by photo-ionization and charge transfer with the ambient ions in the E region of the ionosphere. In the case of the most abundant meteoric metal Fe:

$$Fe + h\nu \rightarrow Fe^+ + e^- \qquad \text{(R1)}$$

$$Fe + NO^+ \rightarrow Fe^+ + NO \qquad \text{(R2)}$$

$$Fe + O_2^+ \rightarrow Fe^+ + O_2 \qquad \text{(R3)}$$

This chemistry is illustrated schematically in Figure 1. Under typical daytime conditions at 100 km, the lifetime against ionization is more than a day.[7] Neutralization of Fe^+ in the MLT occurs in two ways. The first is through formation of a molecular ion, followed by dissociative recombination (DR) with an electron.[8] Fe^+ reacts with O_3, O_2 and N_2:[9]

$$Fe^+ + O_3 \rightarrow FeO^+ + O_2 \qquad \text{(R4)}$$

$$Fe^+ + O_2 (+M) \rightarrow FeO_2^+ \qquad \text{(R5)}$$

$$Fe^+ + N_2 (+M) \rightarrow Fe^+.N_2 \qquad \text{(R6)}$$

where M is a third body (N_2 or O_2). R5 and R6 are pressure-dependent reactions and become faster than R4 below about 90 km,[9] but the resulting FeO_2^+ and $Fe^+.N_2$ ions are rapidly

converted to FeO^+ by reaction with atomic O.[10] As shown in Figure 1, there is then competition between DR:

$$FeO^+ + e^- \rightarrow Fe + O \quad \text{(R7)}$$

and reaction with atomic O

$$FeO^+ + O \rightarrow Fe^+ + O_2 \quad \text{(R8)}$$

which recycles back to Fe^+ and hence prevents neutralization.[10]

The second way in which Fe^+ can be neutralized in the MLT is through radiative and dielectronic recombination:[11]

$$Fe^+ + e^- \rightarrow Fe + h\nu \quad \text{(R9)}$$

Dielectronic recombination (where a free electron is captured and simultaneously excites a core electron of the ion) is a significant process for Fe^+ because the ^6D_J ground state has fine-structure splitting.[12] In fact, the combination of radiative and dielectronic recombination of Fe^+ is relatively inefficient at the low temperatures of the MLT, with a rate coefficient calculated from the R-matrix method to be 8×10^{-12} cm^3 $molecule^{-1}$ s^{-1} at 200 K.[11] However, above 120 km there is essentially no O_3, the atmospheric pressure is very low and the kinetic temperature is high so that molecular ions do not form readily via R4 - R6. In this region, radiative and dielectronic recombination explain the small concentrations of neutral Fe that have recently been observed up to 190 km.[13]

Sporadic E layers are thin layers of highly concentrated plasma consisting of metallic ions - mainly Fe^+ - and electrons, which affect radio wave propagation.[1,2] Lidar observations have revealed the phenomenon of sporadic neutral Fe layers, which often appear explosively below 100 km and can last for several hours.[14] There is a strong statistical correlation in space and time between sporadic E and the appearance of these neutral Fe layers, which has

led to the proposal that sporadic Fe layers are triggered when sporadic E layers descend below about 100 km and the neutralisation of Fe^+ becomes rapid.[14] Thus the chemical lifetime of sporadic E layers, and an explanation for sporadic Fe layers, require a complete understanding of the neutralization pathways of Fe^+.

In the present study we investigate the DR of FeO^+ (highlighted in red in Figure 1). This is the only reaction in the sequence R1 - R8 that has not been studied previously. In fact, apart from two studies of the DR of Na^+ clusters,[15,16] there appear to have been no other studies of DR reactions involving metal-containing ions.[17] It should be noted that theoretical calculations of DR cross sections increase exponentially in complexity with the number of electrons in the molecular ion. DR usually proceeds with an electron being first captured in a high energy Rydberg state, prior to diabatic curve crossing to the dissociative state of the neutral molecule.[17] The number of high-lying Rydberg states for a molecule like FeO prohibits calculation of a complete set of potential energy surfaces, and so experimental measurement is the only realistic approach. Here we report the first measurement of $k_7(FeO^+ + e^-)$, and then examine the impact of this reaction on the lifetime of Fe^+ in the MLT.

2. Experimental

Figure 2 is a schematic diagram of the flowing afterglow apparatus. The stainless steel flow tube is of inner radius 17.5 mm and length 746 mm. A plasma was created by flowing He (4 Standard Litres per Minute (slm) at 1 Torr) through a microwave discharge cavity (McCarroll cavity, 140 W at 2450 MHz) and then injected at the upstream end of the flow tube, where it was immediately mixed with Ar (Ar:He = 1:10) to convert He^+ and any metastable $He(^3P)$ atoms present in the plasma into Ar^+ ions.[18] As a result of the removal of metastable atoms and the large collision cross section of He, the plasma should have cooled down to ~300 K

within 100 mm of the plasma injection point.[18] The electron density of the resulting Ar^+ plasma was measured with a Langmuir probe (Hiden ESPION, with a tungsten tip that is 10 mm long and 0.15 mm in radius). The ESPION software uses the Orbital Motion Limited theory to calculate the electron density.[19] The typical electron density at the point of the Langmuir probe, 337 mm downstream of the plasma injection point, was around 1×10^{10} cm^{-3}. Fe^+ and FeO^+ ions were then introduced into the gas mixture via the ablation of a pure iron rod which was attached to an external rotary drive. The tip of the rod was situated centrally in the laminar gas flow and ablated by a Nd:YAG laser (Continuum Surelite, wavelength = 532 nm, pulse energy = 8 mJ per pulse, pulse rate = 10 Hz), loosely focused onto the rod through an orthogonal side-arm by a 150 mm lens. The rod was rotated (2 - 4 Hz) in order to ensure that a fresh surface of the rod was presented to each successive laser shot. This was necessary to keep the resulting pulses of ablated Fe species as uniform as possible.

A Roots blower (BOC Edwards, Model EH500A) backed by a rotary pump (BOC Edwards, Model E2M80) drew the gas down the flow tube, setting up a laminar flow with the Reynolds number between 200 and 300 (criterion for laminar flow is below 2000) controlled by a throttle valve situated on the exhaust. In these experiments the pressure in the flow tube was maintained at 1.00 Torr, with gas flow velocities ranging from 67.5 – 105.7 m s^{-1}.

Concentrations of the ions in the plasma were analysed by a differentially-pumped quadrupole mass spectrometer (Hiden HPR60) at the downstream end of the flow tube. The mass spectrometer was run in positive ion mode. The skimmer cone between the flow tube and the first stage of the mass spectrometer had a 0.4 mm orifice biased at -17 V, and the skimmer cone between the first and second stage of the mass spectrometer had a 1.8 mm orifice biased at -86 V. Time-resolved ion pulses were captured with a multichannel scaler (EG&G Ortec Model 914P; 5 ns resolution) synchronised to the Q-switch of the Nd:YAG laser. A channel resolution of 100 μs was sufficient to capture the ion pulse shapes in these

ablation experiments. After an initial 10 minutes of ablation, the FeO^+ signal showed no temporal drift over the course of an experiment (typically 90 minutes). In order to obtain an FeO^+ pulse shape for subsequent analysis, FeO^+ pulses from 500 individual laser shots were signal-averaged. The reproducibility of repeat 500 pulse averages was better than 9%.

Materials: He (99.995%, BOC Gases) was purified by passing through a trap of dry molecular sieve (4A, 1-2 mm, Alfa Aesar). Ar (99.9999%, BOC Gases) and O_2 (99.999%, BOC Gases) were used without further purification. N_2O (99.99%, BOC Gases) was purified with three freeze-pump-thaw cycles. The Fe rod used for ablation was 99.95% pure (Alfa Aesar).

3. Results

3.1 Diffusion

A significant difference between the setup used here and previous DR measurements is that the Langmuir probe is fixed in position relative to the flow; it is able to be retracted from the flow into a side arm, but only measures electron density at one point in the flow tube. The mass spectrometer and the iron rod are also fixed in place. The result of this is that the only way to sample the concentrations of electrons and ions at different times during the reaction is to vary the flow rate of the bath gas while maintaining a constant pressure. Figure 3 illustrates the absolute electron density decrease due to ambipolar diffusion to the walls in the Ar^+ plasma, which is well fitted by a single exponential decay and enables the electron density to be extrapolated to flow times outside of the range directly accessible by the Langmuir probe.

The diffusion coefficient for an ion X^+ in He can be obtained from the equation

$$D_{X^+} = k_{loss} P \left(\frac{r^2}{5.81} \right) \qquad \text{(E1)}$$

where k_{loss} is the first-order loss rate in the absence of any reagents, P is the He pressure, and r the radius of the tube.[20] For the example in Figure 3 where $k_{diff} = 794 \pm 43\ s^{-1}$, $D_{Ar+} = 419 \pm 23\ s^{-1}$ Torr $cm^2\ s^{-1}$ at 298 K. The diffusion coefficient can be calculated using the expression[21]

$$D_{X^+} = \frac{k_B T}{2.210 \pi \mu n} \sqrt{\frac{\mu}{\alpha e^2}} \qquad \text{(E2)}$$

where α is the polarizability of the bath gas (0.205 $Å^3$ for He, 1.66 $Å^3$ for Ar [22]), μ is the reduced mass of the X^+ - He(Ar) collision, n the He(Ar) number density, k_B the Boltzmann constant, and e the elemental charge. This gives $D_{Ar+-He} = 347$ and $D_{Ar+-Ar} = 52$ Torr $cm^2\ s^{-1}$ at 298 K. The overall diffusion coefficient in the Ar^+ plasma is then given by

$$D = \frac{D_{He} D_{Ar}}{D_{He} \chi_{Ar} + D_{Ar} \chi_{He}} \qquad \text{(E3)}$$

where χ is the mole fraction of each bath gas ($\chi_{He} = 0.909$; $\chi_{Ar} = 0.091$). This yields D = 229 Torr $cm^2\ s^{-1}$, whereas the measured value is a factor of 1.83 ± 0.10 times higher. The ions in the plasma should diffuse at twice the rate of ions in a neutral gas because of ambipolar diffusion, where the lighter, more mobile electrons effectively pull the ions to the flow tube walls, retaining overall a state of quasi-neutrality. The electrons should then diffuse at a rate close to that of the dominant ion (Ar^+ in these experiments). Note that equation E1 assumes that ions/electrons striking the flow tube walls are removed with 100% efficiency; since this may not be case, particularly if the walls become coated with a non-conducting oxide, then the measured diffusion coefficient will be a lower limit and this probably explains the small

discrepancy between 1.83 and 2. Ambipolar diffusion will be faster than twice the rate of diffusion of ions in a neutral gas if the electron temperature, T_e, is higher than the ion temperature. [23] However in this case, the fact that the measured diffusion coefficient is slightly less than twice the rate of the ion-neutral diffusion confirms that the system was thermally equilibrated at the point where the plasma reached the Langmuir probe.

3.2 DR of N_2O^+ and O_2^+

In order to test the experimental system, one experiment was performed on an N_2O^+ plasma with the Langmuir probe mounted axially in place of the mass spectrometer at the end of the flow tube. This enabled the electron density to be measured up to the point of injection of N_2O. A large excess of N_2O was injected through a 'showerhead' type injector (Figure 2), which is a radially symmetric tubular loop (6 mm OD) with many small holes for rapid mixing of N_2O into the plasma in order to reduce the mixing time.[24] The resulting N_2O^+ ions undergo ambipolar diffusion to the walls and DR:

$$N_2O^+ + e^- \rightarrow \text{products} \qquad \text{(R10)}$$

Figure 4 illustrates the decay of electrons due to both DR (second-order kinetics) and diffusion, both of which are included in a model (see below for more details). A model fit (solid line in Figure 4) yields

$$k_{10}(N_2O^+ + e^-) = (3.3 \pm 0.8) \times 10^{-7}\ \text{cm}^3\ \text{molecule}^{-1}\ \text{s}^{-1}$$

where the error is the standard deviation from 3 data sets (averaging 7 measurements each). Table 1 shows that this result compares satisfactorily with previous measurements.

A second test was then performed to measure the DR rate coefficient of O_2^+ ions

$$O_2^+ + e^- \rightarrow \text{products} \qquad \text{(R11)}$$

under conditions where the O_2^+ is in a large excess of Ar^+ and electrons, thereby simulating the conditions for the FeO^+ DR experiment. Small concentrations of O_2 were added through the shower-head injector to produce O_2^+ via the charge exchange reaction

$$O_2 + Ar^+ \rightarrow O_2^+ + Ar \qquad \text{(R12)}$$

where k_{12} lies in the range (4.9 - 6.0) × 10^{-11} cm^3 $molecule^{-1}$ s^{-1} at 300 K.[25,26] The chemistry of O_2^+, Ar^+ and e^- in the flow tube is described by the following coupled differential equations:

$$\frac{d[O_2^+]}{dt} = k_{12}[Ar^+][O_2] - \left(k_{diff}^{O_2^+} + k_{11}[e^-]\right)[O_2^+] \qquad \text{(E4)}$$

$$\frac{d[Ar^+]}{dt} = -\left(k_{diff}^{Ar^+} + k_{12}[O_2]\right)[Ar^+] \qquad \text{(E5)}$$

$$\frac{d[e^-]}{dt} = -\left(k_{diff}^{e^-} + k_{11}[O_2^+]\right)[e^-] \qquad \text{(E6)}$$

These equations were solved using a fourth-order Runge–Kutta integrator, and k_{11} was determined from a least squares fit to a set of experimental points obtained over a range of Ar^+/e^- concentrations (2.2 × 10^8 - 1.4 × 10^{10} cm^{-3}) at the point of O_2 injection, O_2 concentrations (5.8 × 10^9 - 1.0 × 10^{10} cm^{-3}) and reaction times (3.3 - 7.9 ms). Figure 5 illustrates the measured and modelled $[O_2^+]/[Ar^+]$ ratio over this range of concentration parameter space, plotted against reaction time. Setting k_{12} to 5.5 × 10^{-11} cm^3 $molecule^{-1}$ s^{-1}, which is a mean of previous measurements (see above), the best fit yields

$$k_{11}(O_2^+ + e^-, 298\ K) = (2.0 \pm 0.5) \times 10^{-7}\ cm^3\ molecule^{-1}\ s^{-1}$$

where the quoted error includes an assigned ± 15% uncertainty in k_{12}. Inspection of Table 1 shows that the value for k_{11} obtained in the present study is in very good agreement with previous measurements.[25,27,28]

3.3 DR of FeO^+

Initially, FeO^+ was produced from Fe^+ by adding N_2O downstream of the ablation source:[9]

$$Fe^+ + N_2O \rightarrow FeO^+ + N_2 \qquad \text{(R13)}$$

However, addition of N_2O greatly increases the complexity of the system because it undergoes charge transfer with Ar^+ and the resulting N_2O^+ both removes electrons and converts FeO from the ablation source into FeO^+. It also clusters readily with Fe^+ and FeO^+.[29]

In fact, it was then found that there was sufficient oxidation of the surface of the Fe rod (when exposed routinely to air) that FeO^+ was produced directly by ablation, so addition of N_2O was not required. Figure 6 illustrates a sequence of time-resolved FeO^+ pulses measured at the downstream end of the flow tube for a range of flow velocities (or flow times, since the pressure is constant). One significant advantage of the pulsed ablation system is that the arrival time of the pulses gives a direct measure of the axial flow velocity in the tube, rather than using the mass flow rates and pressure to calculate the plug flow velocity and applying a laminar flow correction.[30] In practice, this latter procedure for calculating the flow velocity, which had to be used for the study of N_2O^+ and O_2^+ described above, always agreed to within 8% of the direct measurement.

The iron species generated via ablation include not only Fe^+ and FeO^+ ions, but also neutral Fe and FeO.[31] Resonance absorption measurements, performed transverse to the flow tube axis with a Fe hollow cathode lamp,[31] showed that the Fe concentration was less than 10^9 cm^{-3}. Charge transfer between Ar^+ and neutral FeO is an additional source of FeO^+:

$$Ar^+ + FeO \rightarrow FeO^+ + Ar \qquad \text{(R14)}$$

The rate coefficient for this reaction was estimated using modified Langevin theory,[32,33] because FeO has a significant dipole moment of 4.5 D,[34] yielding $k_{14}(Ar^+ + FeO, 298\ K) = 4.4 \times 10^{-9}\ cm^3\ molecule^{-1}\ s^{-1}$.

The chemistry of FeO^+, FeO, Ar^+ and e^- in the flow tube is described by the following coupled differential equations:

$$\frac{d[FeO^+]}{dt} = k_{14}[Ar^+][FeO] - \left(k_{diff}^{FeO^+} + k_7[e^-]\right)[FeO^+] \qquad \text{(E7)}$$

$$\frac{d[FeO]}{dt} = -\left(k_{diff}^{FeO} + k_{14}[Ar^+]\right)[FeO] \qquad \text{(E8)}$$

$$\frac{d[Ar^+]}{dt} = -\left(k_{diff}^{Ar^+} + k_{14}[FeO]\right)[Ar^+] \qquad \text{(E9)}$$

$$\frac{d[e^-]}{dt} = -\left(k_{diff}^{e^-} + k_7[FeO^+]\right)[e^-] \qquad \text{(E10)}$$

The electron diffusion rate k_{diff}^{e-} averaged 815 s^{-1} at 1.0 Torr, measured by the Langmuir probe. The diffusion rate of Ar^+, the dominant positive charge carrier was assumed to match the electron diffusion rate, and that of FeO^+ was scaled using the relative diffusion coefficients calculated with equation E2. Since the reduced masses of the ion-neutral pairings are very similar, the diffusion rate of FeO^+ is 3% smaller than that of Ar^+. The diffusion rate of neutral FeO was calculated to be 401 s^{-1} in the flow tube.[31]

Equations E7 - E10 were solved numerically to predict the relative FeO^+ concentration at the downstream end of the flow tube. The two unknowns are k_7 and $[FeO_0]$, the initial neutral FeO concentration produced by ablation of the Fe rod. By repeating the model runs over a wide range of flow velocities (67.5 - 105.7 m s^{-1}) and electron densities (8.1×10^8 - 9.2×10^9 cm^{-3}) and comparing with the measured FeO^+ signal, a χ^2 goodness-of-fit parameter was calculated for N experimental points in a data set:

$$\chi^2 = \sum_{i=1}^{N} \left(\frac{\left(FeO^+_{expt,i} - FeO^+_{model,i} \right)}{FeO^+_{expt,i}} \right)^2 \qquad \text{(E11)}$$

A Nelder-Mead iteration algorithm[35] was then used to find the optimal values of k_7 and $[FeO_0]$. Note that in order to model the time-resolved FeO^+ concentration, the model actually requires the product $k_{14}[FeO]$ in equation E7; since we fix k_{14} to the calculated value, $[FeO_0]$ is then the other unknown fitted parameter. Figure 7 is an example of the results of a single experiment. Panels (a) and (b) compares the measured and modelled FeO^+ signals as a function of velocity and initial electron density (t = 0 being defined as the time when the plasma passes the iron rod). The dotted lines in both panels show how FeO^+ would have varied in the absence of DR, showing that DR makes a significant difference to the measured FeO^+ signal. Figure 7(c) is a contour plot of χ^2 as a function of k_7 and $[FeO_0]$. The minimum of the χ^2 surface is marked with a white cross. In this case $k_7 = (4.5 \pm 1.8) \times 10^{-7}$ cm^3 $molecule^{-1}$ s^{-1}. The error was estimated by using Monte Carlo selection of the following model parameters within their percentage uncertainties indicated in parentheses: FeO^+ produced directly by ablation (±20%); initial electron density (±10%); and flow velocity (±0.3%). The kinetic model was then rerun to obtain new optimised fits of k_7 and $[FeO_0]$ to the experimental data points. The standard deviation of k_7 from 10^3 model fits then provided

the estimate of the uncertainty. The grey envelope in Figure 7(a) and (b) indicates the uncertainty in the fit predicted from this Monte Carlo procedure.

Eleven such experimental data-sets were obtained, with k_7 varying from 4.0×10^{-7} cm^3 $molecule^{-1}$ s^{-1} to 7.2×10^{-7} cm^3 $molecule^{-1}$ s^{-1}. The largest random error arises from extrapolating the electron density along the flow tube using the measured value of k_{diff}^{e-}, and this is likely responsible for the range of k_7 retrieved from the χ^2 minimization. The average value from these 11 individual experiments is

$$k_7(FeO^+ + e^-, 298\ K) = (5.5 \pm 1.0) \times 10^{-7}\ cm^3\ molecule^{-1}\ s^{-1}$$

where the quoted error is the 2σ standard deviation. The average fitted value for $[FeO_0]$ is $(3.7 \pm 1.0) \times 10^7$ molecule cm^{-3}.

4. Discussion

The measured value of k_7 is 2 - 3 times larger than the rate coefficients typical of DR reactions involving diatomic ions,[17] exemplified by the O_2^+ DR reaction measured here (k_{11}). This probably reflects the high density of FeO Rydberg states that will be involved in the reaction. k_7 is also roughly twice as large as the value that that has been used in atmospheric models of meteoric Fe.[7,8,36] A comprehensive review shows that DR reactions tend to have a small negative temperature dependence, which can be expressed as T^{-n} with n between 0.5 and 1.[17] If n were 0.5 then k_7 would be only 22% higher at 200 K, a typical mesospheric temperature. While the experimental temperature range of the flow tube could be extended to 200 K as we have done previously,[37] it would not be possible to measure a difference of only ~20% in k_7, given the additional uncertainties with the temperature dependences of other parameters in the kinetic model. Here we assume a $T^{-0.5}$ dependence.

We now consider the impact of the FeO^+ DR reaction on the lifetime of Fe^+ in the MLT region. As discussed in the Introduction and illustrated in Figure 1, reaction R7 is the key reaction for neutralizing Fe^+ so long as there is sufficient O_3 to form FeO^+ via reaction R4, although the overall efficiency of this process is controlled by atomic O (reaction R8). Putting FeO^+ in steady-state yields the first-order rate of Fe^+ conversion to Fe:

$$\text{DR rate}(Fe^+ \rightarrow Fe) = k_4[O_3]\frac{k_7[e^-]}{k_7[e^-]+k_8[O]} \qquad \text{(E12)}$$

$$\approx k_4[O_3]\frac{k_7[e^-]}{k_8[O]} \quad \text{since } k_7[e^-] << k_8[O]$$

The rate of neutralisation via radiative recombination (RR) is $k_9[e^-]$. Figure 8 illustrates vertical profiles of the DR and RR rates in the MLT, for daytime and night-time at 40^oN in March. The vertical profiles of the relevant atmospheric constituents (O_3, O, e^-) are taken from the Whole Atmosphere Community Climate Model (WACCM).[38] Note the large increase of the RR rate in the daytime, when photo-ionization leads to a more than 10-fold increase in electrons. In contrast, there is little diurnal change in the DR rate, because the roughly 10-fold decrease in O_3 caused by photolysis during daytime is roughly balanced by the increase in electron density through photo-ionization, and the DR rate is proportional to $[O_3]$ $[e^-]$ since [O] does not exhibit significant diurnal variation above 85 km.[7] During daytime, DR is more important than RR below about 102 km; whereas at night, this transition occurs around 108 km. The top abscissa of the plot in Figure 10 shows the lifetime of Fe^+. Note that the atomic ion is very long-lived (more than 1 day) above 95 km. However, if the metallic ions and electrons become concentrated into a sporadic E layer where the electron density can exceed 10^5 cm^{-3}, then the lifetime will decrease to only a few minutes.[10]

We have recently developed a global atmospheric model of meteoric iron (WACCM-Fe).[36] The model includes the seasonally varying meteoric injection rate profile of Fe and a detailed description of the neutral and ion-molecule chemistry of iron, incorporated into the WACCM chemistry-climate model. WACCM-Fe simulates the mesospheric Fe atom layer satisfactorily, particularly for northern mid-latitudes.[36] However, in that modeling study the high sensitivity to k_7 of the underside of the Fe^+ ion layer was identified using a 1D model. We have now rerun the full 3D model simulation using the measured value for k_7 with an assumed $T^{-0.5}$ dependence. Figure 9 shows the vertical profile Fe^+ measured over Red Lake (51^oN, 267^oE), Canada using a rocket-borne mass spectrometer during daytime.[39] Note how the Fe^+ density increases extremely rapidly by over 3 orders of magnitude between 80 km and the peak around 95 km, before decreasing again above 100 km. Plotted for comparison are two WACCM simulations for similar conditions (solar maximum year), using the previously assumed value of k_7 and the larger value measured in this study. Clearly, the model run with the new value of k_7 captures the very small scale height on the underside of the layer and the Fe^+ peak density very well, whereas the smaller value of k_7 used previously causes the peak density to be overpredicted by a factor of ~3. Note that the discrepancy between both WACCM simulations and the measurements above 100 km appears to be due to an incomplete description in WACCM of electrodynamic transport in the thermosphere.[36] Specifically, WACCM does not include the Lorentz force, which manifests as an upward drift of ions when an eastward wind transports through them through the Earth's magnetic field. This can result in significant upward transport of a long-lived species such as Fe^+ above 100 km.[40]

5. Conclusions

In this study we have reported the first measurement of the rate coefficient for the DR of FeO^+ with electrons. The rate coefficient is roughly double the "typical" value assumed for the DR reactions of diatomic molecular ions, probably as a result of the high density of Rydberg states in FeO which are likely to be involved in the reaction. The most important reactions which govern the reduction of Fe^+ to Fe in the upper mesosphere and lower thermosphere have now been measured, which should lead to better quantitative prediction of the chemical lifetime of sporadic E layers and their effect on radio propagation.

Acknowledgments. This work was supported by the European Research Council (project number 291332 - CODITA).

References

(1) Grebowsky, J. M.; Aikin, A. C. In situ measurements of meteroric ions. In Meteors in the Earth's Atmosphere; Murad, E., Williams, I. P., Eds.; Cambridge University Press: Cambridge, 2002.

(2) Kopp, E. On the abundance of metal ions in the lower ionosphere, J. Geophys. Res.-Atmos. **1997**, 102, 9667-9674.

(3) Anderson, J. G.; Barth, C. A. Rocket investigation of Mg I and Mg II dayglow, J. Geophys. Res.-Atmos. **1971**, 76, 3723-3729.

(4) Gardner, J. A.; Broadfoot, A. L.; McNeil, W. J.; Lai, S. T.; Murad, E. Analysis and modeling of the GLO-1 observations of meteoric metals in the thermosphere, J. Atmos. Solar-Terr. Phys. **1999**, 61, 545-562.

(5) Langowski, M.; Savigny, C. v.; Burrows, J. P.; Feng, W.; Plane, J. M. C.; Marsh, D. R.; Janches, D.; Sinnhuber, M.; Aikin, A. C. Global investigation of the Mg atom and ion layers using SCIAMACHY/Envisat observations between 70 km and 150 km altitude and WACCM-Mg model results, Atmos. Chem. Phys. **2015**, 15, 273-295.

(6) Gerding, M.; Alpers, M.; von Zahn, U.; Rollason, R. J.; Plane, J. M. C. Atmospheric Ca and Ca^+ layers: midlatitude observations and modeling, J. Geophys. Res.-Atmos. **2000**, 105, 27131-27146.

(7) Plane, J. M. C.; Feng, W.; Dawkins, E. C. M. The mesosphere and metals: chemistry and changes, Chem. Rev. **2015**, DOI: 10.1021/cr500501m.

(8) Helmer, M.; Plane, J. M. C.; Qian, J.; Gardner, C. S. A model of meteoric iron in the upper atmosphere, J. Geophys. Res.-Atmos. **1998**, 103, 10913-10925.

(9) Vondrak, T.; Woodcock, K. R. I.; Plane, J. M. C. A kinetic study of the reactions of Fe^+ with N_2O, N_2, O_2, CO_2 and H_2O, and the ligand-switching reactions $Fe^+.X + Y \rightarrow Fe^+.Y + X$ ($X = N_2$, O_2, CO_2; $Y=O_2$, H_2O), Phys. Chem. Chem. Phys **2006**, 8, 503-512.

(10) Woodcock, K. R. S.; Vondrak, T.; Meech, S. R.; Plane, J. M. C. A kinetic study of the reactions $FeO^+ + O$, $Fe^+.N_2 + O$, $Fe^+.O_2 + O$ and $FeO^+ + CO$: implications for sporadic E layers in the upper atmosphere, Phys. Chem. Chem. Phys **2006**, 8, 1812-1821.

(11) Nahar, S. N.; Bautista, M. A.; Pradhan, A. K. Electron-ion recombination of neutral iron, Astrophys. J. **1997**, 479, 497-503.

(12) Bryans, P.; Kreckel, H.; Roueff, E.; Wakelam, V.; Savin, D. W. Molecular cloud chemistry and the importance of dielectronic recombination, Astrophys. J. **2009**, 694, 286–293.

(13) Chu, X.; Yu, Z.; Gardner, C. S.; Chen, C.; Fong, W. Lidar observations of neutral Fe layers and fast gravity waves in the thermosphere (110-155 km) at McMurdo (77.8^o S, 166.7^o E), Antarctica, Geophys. Res. Lett. **2011**, 38, L23807.

(14) Alpers, M.; Höffner, J.; von Zahn, U. Sporadic Fe and E layers at polar, middle, and low latitudes, J. Geophys. Res.-Atmos. **1994**, 99, 14971-14985.

(15) Zhaunerchyk, V.; Ehlerding, A.; Geppert, W. D.; Hellberg, F.; Thomas, R. D.; Larsson, M.; Viggiano, A. A.; Arnold, S. T.; Osterdahl, F.; Hlavenka, P. Dissociative recombination study of $Na^+(D_2O)$ in a storage ring, J. Chem. Phys. **2004**, 121, 10483-10488.

(16) Keller, G. E.; Beyer, R. A. CO_2 and O_2 clustering to sodium ions, J. Geophys. Res.-Atmos. **1971**, 76, 289-290.

(17) Florescu-Mitchell, A. I.; Mitchell, J. B. A. Dissociative recombination, Phys. Rep. Rev. Phys. Lett. **2006**, 430, 277-374.

(18) Smith, D.; Adams, N. G.; Dean, A. G.; Church, M. J. Application of Langmuir probes to study of flowing afterglow plasmas, J. Phys. D - Appl. Phys. **1975**, 8, 141-152.

(19) Mott-Smith, H. M.; Langmuir, I. The theory of collectors in gaseous discharges, Phys. Rev. **1926**, 28, 0727-0763.

(20) Cox, R. M.; Plane, J. M. C. An experimental and theoretical study of the clustering reactions between Na^+ ions and N_2, O_2 and CO_2, J. Chem. Soc. Faraday Trans. **1997**, 93, 2619-2629.

(21) Rees, M. H. Physics and chemistry of the upper atmosphere; Cambridge University Press: Cambridge, 1989.

(22) Lide, D. R. Handbook of Physics and Chemistry; CRC Press: Boca Raton, FL, 1992; Vol. 72nd edn.

(23) Smirnov, B. R. Physics of ionized gases; John Wiley & Sons: Chichester, 2001.

(24) Alge, E.; Adams, N. G.; Smith, D. Measurements of the dissociative recombination coefficients of O_2^+, NO^+ and NH_4^+ in the temperature range 200-600 K, J. Phys. B - At. Mol. Opt. Phys. **1983**, 16, 1433-1444.

(25) Anicich, V. G. An index of the literature for bimolecular gas phase cation-molecule reaction kinetics, JPL Publication 03-19; Jet Propulsion Laboratory/California Institute of Technology: Pasadena, CA, 2003.

(26) Ziolkowski, M.; Schatz, G. C.; Viggiano, A. A.; Midey, A.; Dotan, I. O_2(X) and O_2(a) charge exchange with simple ions, J. Chem. Phys. **2014**, 140, 214307.

(27) Peverall, R.; Rosen, S.; Peterson, J. R.; Larsson, M.; Al-Khalili, A.; Vikor, L.; Semaniak, J.; Bobbenkamp, R.; Padellec, A. L.; Maurellis, A. N. et al. Dissociative recombination and excitation of O_2^+: cross sections, product yields and implications for studies of ionospheric airglows, J. Chem. Phys. **2001**, 114, 6679-6689.

(28) Fournier, J. A.; Shuman, N. S.; Melko, J. J.; Ard, S. G.; Viggiano, A. A. A novel technique for measurement of thermal rate constants and temperature dependences of dissociative recombination: CO_2^+, CF_3^+, N_2O^+, $C_7H_8^+$, $C_7H_7^+$, $C_6H_6^+$, $C_6H_5^+$, $C_5H_6^+$, $C_4H_4^+$, and $C_3H_3^+$, J. Chem. Phys. **2013**, 138, 154201.

(29) Baranov, V.; Javahery, G.; Hopkinson, A. C.; Bohme, D. K. Intrinsic coordination properties of iron in FeO^+: Kinetics at 294+/-3 K for gas-phase reactions of the ground states of Fe^+ and FeO^+ with inorganic ligands containing hydrogen, nitrogen, and oxygen, J. Am. Chem. Soc. **1995**, 117, 12801-12809.

(30) Brown, R. L. Tubular flow reactors with 1st-order kinetics, J. Res. Nat. Bur. Stand. **1978**, 83, 1–8.

(31) Self, D. E.; Plane, J. M. C. A kinetic study of the reactions of iron oxides and hydroxides relevant to the chemistry of iron in the upper mesosphere, Phys. Chem. Chem. Phys **2003**, 5, 1407-1418.

(32) Troe, J. Statistical adiabatic channel model of the ion neutral dipole capture rate constants, Chem. Phys. Lett. **1985**, 122, 425-430.

(33) Su, T.; Chesnavich, W. J. Parameterization of the ion-polar molecule collision rate constant by trajectory calculations, J. Chem. Phys. **1982**, 76, 5183-5185.

(34) Steimle, T. C.; Gengler, J.; Hodges, P. J. The permanent electric dipole moments of iron monoxide, FeO, J. Chem. Phys. **2004**, 121, 12303-12307.

(35) Nelder, J. A.; Mead, R. A simplex method for function minimization, Comp. J. **1965**, 7, 308-313.

(36) Feng, W. H.; Marsh, D. R.; Chipperfield, M. P.; Janches, D.; Hoffner, J.; Yi, F.; Plane, J. M. C. A global atmospheric model of meteoric iron, J. Geophys. Res.-Atmos. **2013**, 118, 9456-9474.

(37) Broadley, S. L.; Plane, J. M. C. A kinetic study of reactions of calcium-containing molecules with O and H atoms: implications for calcium chemistry in the upper atmosphere, Phys. Chem. Chem. Phys **2010**, 12, 9095-9107.

(38) Marsh, D. R.; Mills, M. J.; Kinnison, D. E.; Lamarque, J.-F.; Calvo, N.; Polvani, L. M. Climate Change from 1850 to 2005 Simulated in CESM1(WACCM), J. Climate **2013**, 26, 7372-7391.

(39) Kopp, E. Mesospheric H_2O andH_2O_2 densities inferred from in situ positive ion composition measurement, Adv. Space Res. **1984**, 4, 13–18.

(40) Rees M.H. Physics and chemistry of the upper atmosphere; Cambridge University Press: Cambridge, 1989.

(41) Hamberg, M.; Geppert, W. D.; Rosen, S.; Hellberg, F.; Ehlerding, A.; Zhaunerchyk, V.; Kaminska, M.; Thomas, R. D.; af Ugglas, M.; Kallberg, A. et al. Branching ratios and

absolute cross sections of dissociative recombination processes of N_2O^+, Phys. Chem. Chem. Phys **2005**, 7, 1664-1668.

Table 1. Rate coefficients for the dissociative recombination of O_2^+ and N_2O^+ with electrons, compare with recent previous measurements (see Anicich[25] for pre-2000 measurements)

	DR rate coefficient, 290 - 300 K (cm^3 $molecule^{-1}$ s^{-1})	Source
$O_2^+ + e^-$	$(2.4 \pm 0.7) \times 10^{-7}$	Peverall et al.[27]
	$(1.9 \pm 0.5) \times 10^{-7}$	Fournier et al. [28]
	$(2.0 \pm 0.5) \times 10^{-7}$	This work
$N_2O^+ + e^-$	$(3.3 \pm 0.8) \times 10^{-7}$	Hamberg et al.[41]
	$(3.0 \pm 0.5) \times 10^{-7}$	Fournier et al. [28]
	$(3.3 \pm 0.8) \times 10^{-7}$	This work

Figure captions.

Figure 1. Reaction scheme illustrating the coupling between Fe^+ and Fe in the mesosphere/lower thermosphere. The reaction highlighted in red is the subject of the present study.

Figure 2. Schematic diagram of the flowing afterglow apparatus. FeO^+ ions are produced by pulsed laser ablation of an iron rod.

Figure 3. Electron density measured by the Langmuir probe (solid symbols) with fitted exponential decay (solid line) to illustrate ambipolar diffusion in the Ar^+ plasma. Experimental conditions: pressure = 1.0 Torr, temperature = 298 K, total flow rate = 3.1 – 4.5 slm, flow velocity 70.3 – 103.0 m s^{-1}. t = 0 refers to the time of injection of plasma from the discharge into the flow tube.

Figure 4. The measured decay of electrons in an N_2O^+ plasma, compared with a model of the second-order DR kinetics and diffusion to the walls. Experimental conditions: pressure = 1.0 Torr, $[N_2O] = 8 \times 10^{13}$ molecules cm^{-3}, temperature = 298 K, total flow rate = 3.08 slm, flow velocity 70.3 m s^{-1}.

Figure 5. Plot of the measured and modelled $[O_2^+] : [Ar^+]$ ratio versus reaction time in a study of the O_2^+ DR reaction. Experimental conditions: pressure = 1.0 Torr, temperature = 298 K, total mass flow rate = 2.2 – 4.0 slm, flow velocity = 58.8 – 104.4 m s^{-1}.

Figure 6. Pulses of FeO^+ ions as a function of flow time, measured by the mass spectrometer/ multichannel scaler for a range of flow velocities. Experimental conditions: pressure = 1.0 Torr, temperature = 298 K, flow velocity 73.0 – 105.7 m s^{-1}.

Figure 7. Plots of fitted and measured concentrations of the FeO^+ signal as a function of flow velocity (panel a) and electron density at the Fe rod (panel b). The fitted rate coefficient is $k_7 = 4.7 \times 10^{-7}$ cm^3 $molecule^{-1}$ s^{-1}. The envelope corresponds to the $\pm 1\sigma$ uncertainty determined

from a Monte Carlo procedure (see text). The dashed line indicates the concentration of FeO^+ that would have been observed if DR were not occurring. Experimental conditions: pressure = 1.0 Torr, T = 298 K, total mass flow rate = 3.2 – 4.6 slm. Panel c is a contour plot of χ^2 as a function of k_7 and the initial concentration of neutral FeO.

Figure 8. Vertical profiles of the daytime and night-time rates of neutralization of Fe^+ via dissociative recombination (DR - black lines) and radiative recombination (RR - blue lines) with electrons (bottom abscissa). The Fe^+ lifetimes (red lines) are shown on the top abscissa. The conditions are March, 40^oN.

Figure 9. Comparison between concentrations of Fe^+ as a function of altitude: measured by rocket-borne mass spectrometry at Red Lake, Canada (51°N, 267°E at 16:52 UT)[39] (diamonds); modeled by Feng et al.[36] (solid line); and modeled using the rate coefficient for $k_7(FeO^+ + e^-)$ measured in the present study (dashed line).

Figure 1.

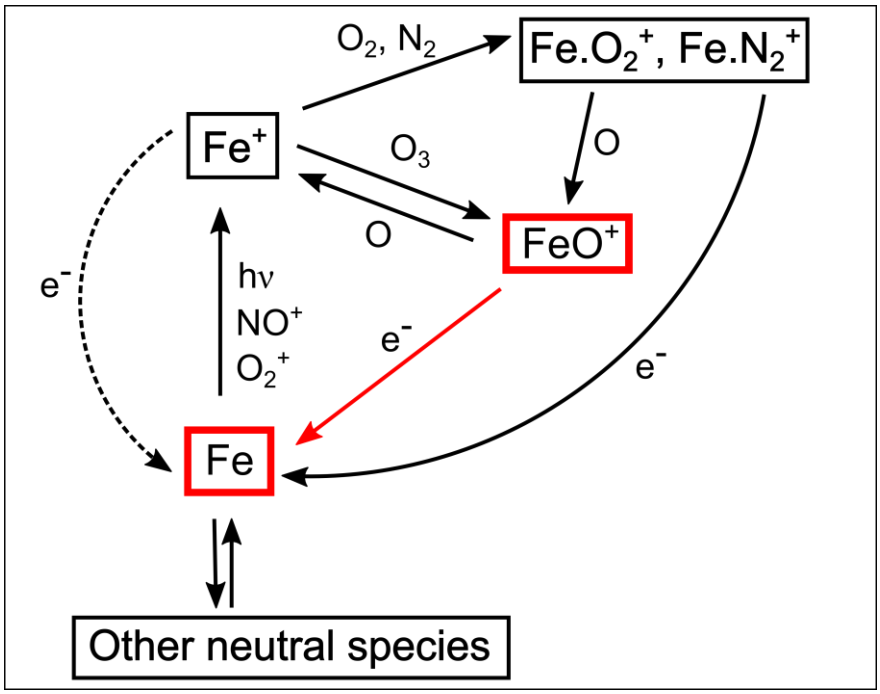

Figure 1. Reaction scheme illustrating the coupling between Fe^+ and Fe in the mesosphere/lower thermosphere. The reaction highlighted in red is the subject of the present study.

Figure 2.

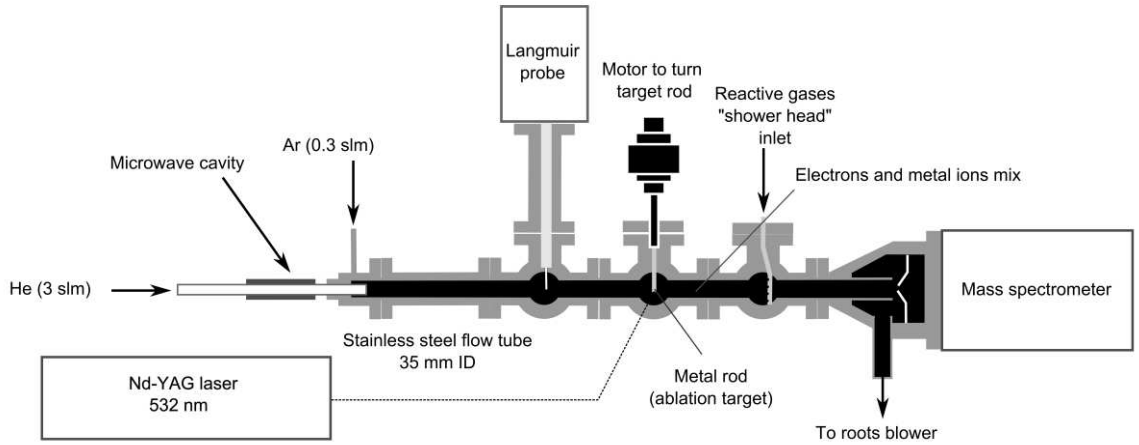

Figure 2. Schematic diagram of the flowing afterglow apparatus. FeO^+ ions are produced by pulsed laser ablation of an iron rod.

Figure 3.

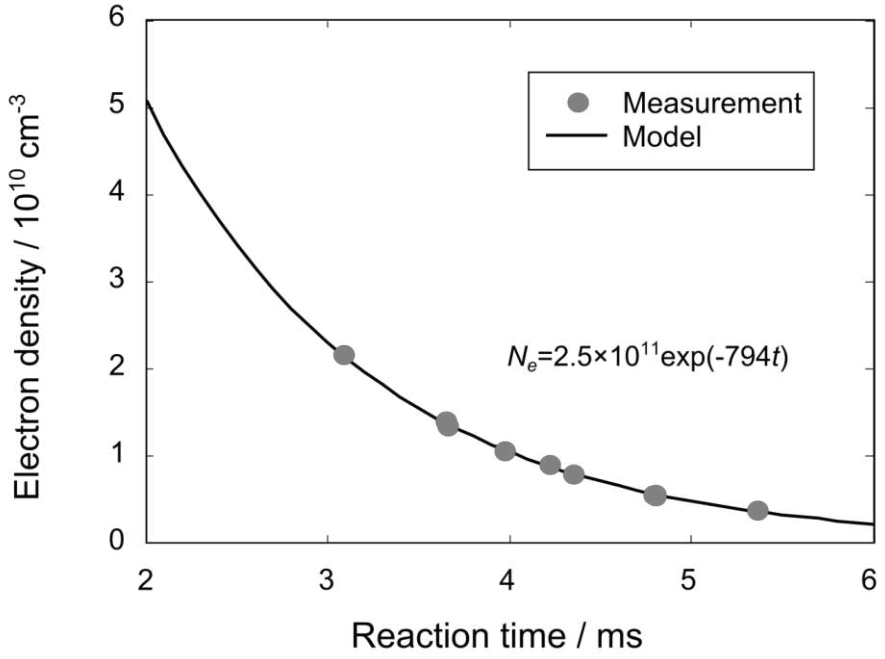

Figure 3. Electron density measured by the Langmuir probe (solid symbols) with fitted exponential decay (solid line) to illustrate ambipolar diffusion in the Ar^+ plasma. Experimental conditions: pressure = 1.0 Torr, temperature = 298 K, total flow rate = 3.1 – 4.5 slm, flow velocity 70.3 – 103.0 m s^{-1}. t = 0 refers to the time of injection of plasma from the discharge into the flow tube.

Figure 4.

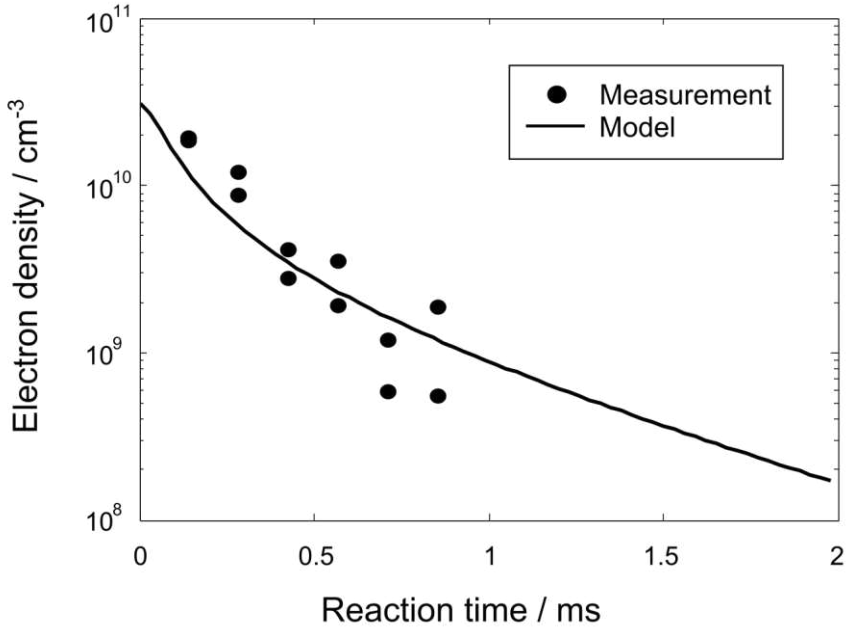

Figure 4. The measured decay of electrons in an N_2O^+ plasma, compared with a model of the second-order DR kinetics and diffusion to the walls. Experimental conditions: pressure = 1.0 Torr, $[N_2O] = 8 \times 10^{13}$ molecules cm^{-3}, temperature = 298 K, total flow rate = 3.08 slm, flow velocity 70.3 m s^{-1}.

Figure 5.

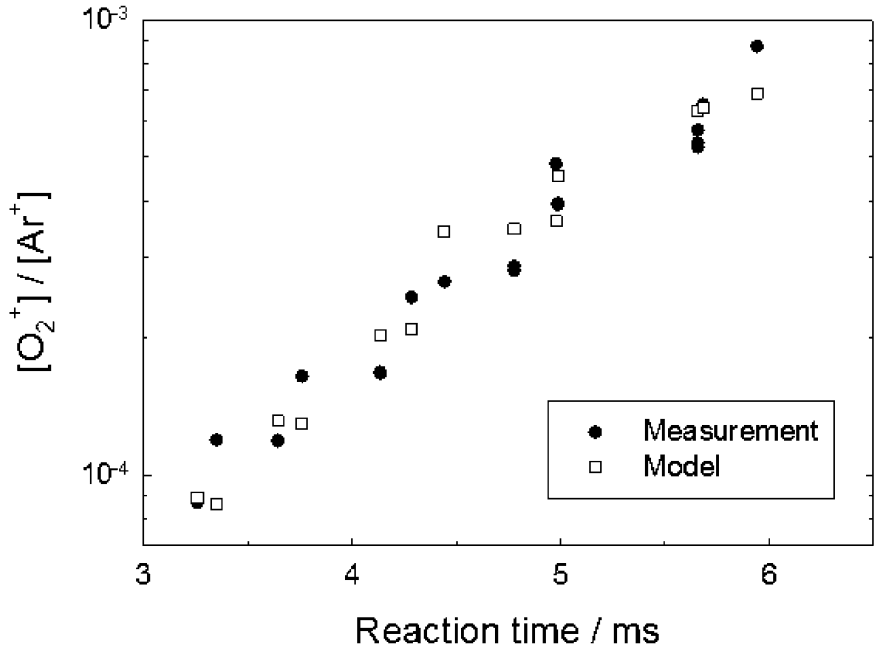

Figure 5. Plot of the measured and modelled $[O_2^+]$: $[Ar^+]$ ratio versus reaction time in a study of the O_2^+ DR reaction. Experimental conditions: pressure = 1.0 Torr, temperature = 298 K, total mass flow rate = 2.2 – 4.0 slm, flow velocity = 58.8 – 104.4 m s^{-1}.

Figure 6.

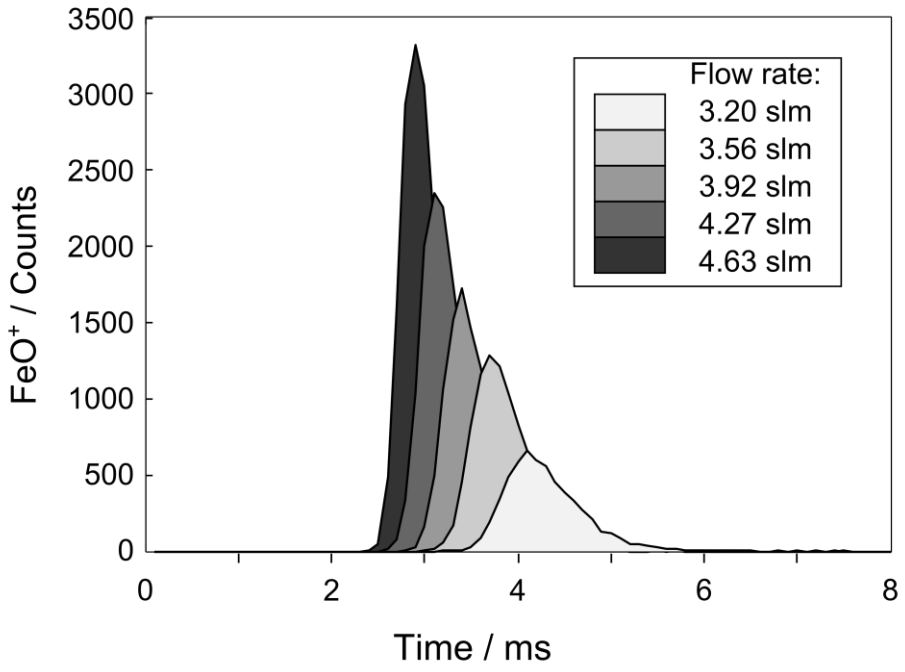

Figure 6. Pulses of FeO^+ ions as a function of flow time, measured by the mass spectrometer/ multichannel scaler for a range of flow velocities. Experimental conditions: pressure = 1.0 Torr, temperature = 298 K, flow velocity 73.0 – 105.7 m s^{-1}.

Figure 7.

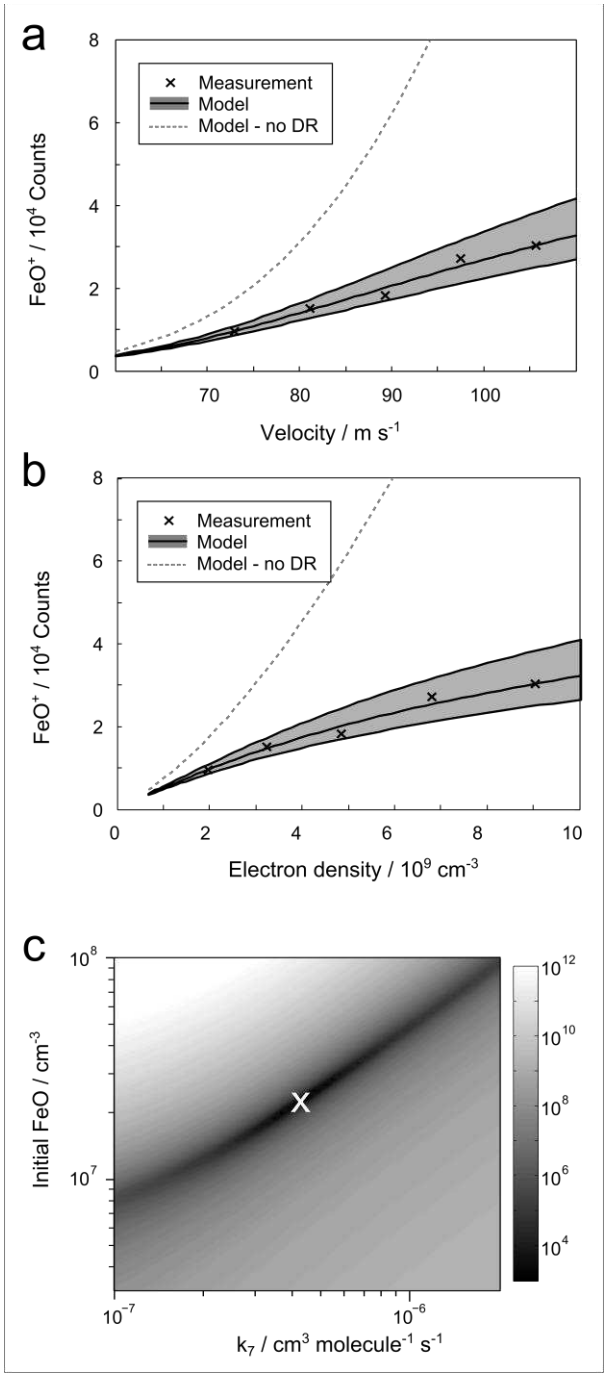

Figure 7. Plots of fitted and measured concentrations of the FeO^+ signal as a function of flow velocity (panel a) and electron density at the Fe rod (panel b). The fitted rate coefficient is $k_7 = 4.7 \times 10^{-7}$ cm^3 molecule^{-1} s^{-1}. The envelope corresponds to the ± 1σ uncertainty determined from a Monte Carlo procedure (see text). The dashed line indicates the concentration of FeO^+ that would have been observed if DR were not occurring. Experimental conditions: pressure = 1.0 Torr, T = 298 K, total mass flow rate = 3.2 – 4.6 slm. Panel c is a contour plot of χ^2 as a function of k_7 and the initial concentration of neutral FeO.

Figure 8.

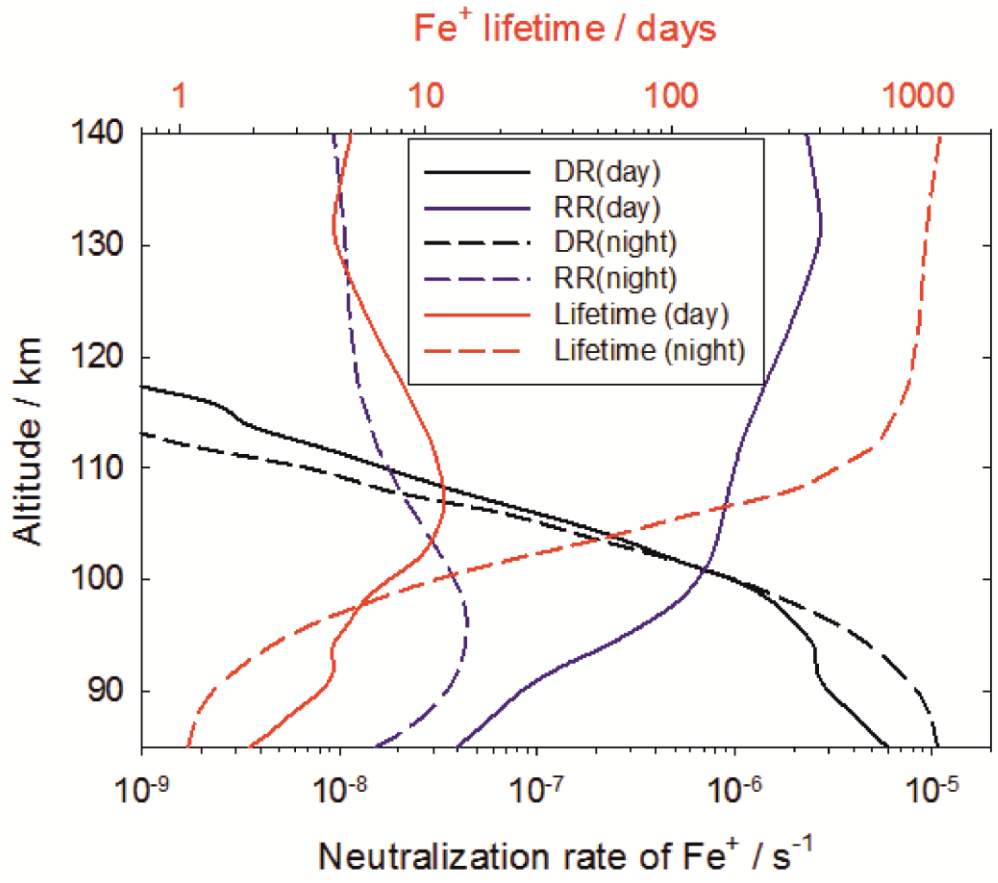

Figure 8. Vertical profiles of the daytime and night-time rates of neutralization of Fe^+ via dissociative recombination (DR - black lines) and radiative recombination (RR - blue lines) with electrons (bottom abscissa). The Fe^+ lifetimes (red lines) are shown on the top abscissa. The conditions are March, 40^oN.

Figure 9.

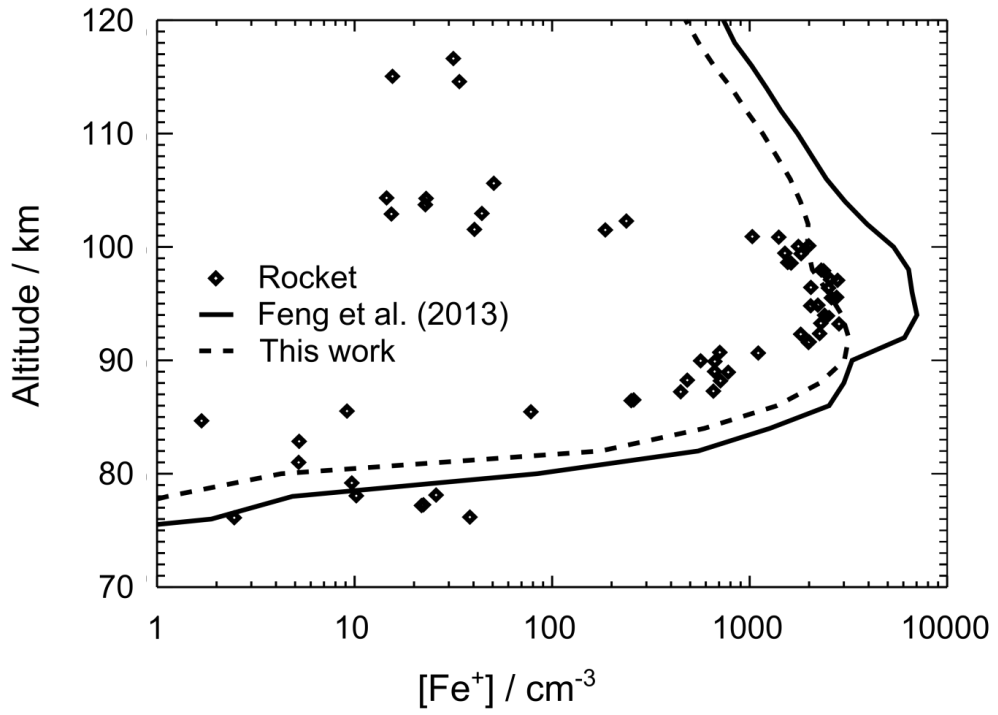

Figure 9. Comparison between concentrations of Fe^+ as a function of altitude: measured by rocket-borne mass spectrometry at Red Lake, Canada (51°N, 267°E at 16:52 UT)[39] (diamonds); modeled by Feng et al.[36] (solid line); and modeled using the rate coefficient for $k_7(FeO^+ + e^-)$ measured in the present study (dashed line).